Electronic Supplementary Information for

Vanadium Hexacyanoferrate as High-Capacity Cathode for Fast Proton Storage

*Xuancheng Peng,[‡] Haocheng Guo,[‡] Wenhao Ren, Zhen Su, Chuan Zhao**

School of Chemistry, University of New South Wales, Sydney, New South Wales 2052, Australia

E-mail: chuan.zhao@unsw.edu.au

Experimental Section

Synthesis of Vanadium Precursor Solution: Vanadium precursor solution was synthesized via a chemical reduction method reported previously with slight modification.[1] Typically, 50 ml 32% HCl was diluted with DI water to 75 ml, to which 4 g V_2O_5 was then added with magnetic stirring to yield a yellow suspension. Afterwards, 700 µl glycerol was added dropwise, and the solution was continuously stirred until a clear blue solution formed. The temperature of the solution was maintained at 60 ℃ throughout.

Synthesis of Vanadium Hexacyanoferrate (VHCF): In a typical procedure (**Figure S1**), as-prepared vanadium precursor solution (9.375 ml) was diluted with DI water to 50 ml under stirring to form a transparent blue solution A. $K_3Fe(CN)_6$ (3.6 mmol) was then dissolved in DI water to generate 50 ml yellow solution B. Thereafter, solution B was dropwise added into solution A with magnetic stirring under 60 ℃ for 9 hours. After cooling to room temperature, centrifuge separation and wash (by DI water and ethanol, three times per agent) were performed to obtain the green precipitates. Finally, the as-prepared precipitates were air-dried under 80 ℃ overnight.

Physical Characterization: Scanning Electron Microscopy (SEM) images were collected by FEI Nova NanoSEM 450. Typically, the sample was dropped onto a Si wafer then sputter coated with carbon. Transmission electron microscope (TEM) bright field images, selected area electron diffraction (SAED) and element mapping were recorded by the JEOL JEM-F200 (200 kV) with an energy dispersive X-ray (EDX) spectroscopy. Fourier Transform Infrared Spectroscopy (FTIR) transmittance spectra were recorded by a PerkinElmer Spotlight FT-IR spectrometer within the range of 600-4000 cm^{-1}. Raman spectra were recorded by a Renishaw INVIA micro-Raman spectroscopy operating at 532 nm diode laser. Otherwise noted, X-ray Diffraction (XRD) of powder samples were performed by the Empyrean diffractometer (Co Kα, 40 mA, 45 kV, Malvern Panalytical) to avoid fluorescent influences of Fe, ex-situ XRD patterns of electrode samples were recorded by the bench-top Aeris diffractometer (Cu Kα, 40 mA, 45 kV, Malvern Panalytical) with reduced reflection path to boost signal recording. All positions were converted to values of the same X-ray wavelength (1.5406 Å, Cu Kα radiation) for clarity. X-ray Photoelectron Spectroscopy (XPS) was carried out via Thermo Scientific ESCALAB250X using mono-chromated Al K alpha (120 W, 20 eV pass energy, 500 µm spot size). Result patterns were calibrated according to reference peak of C 1s at 284.8 eV. Elemental analysis was performed on inductively coupled plasma emission

spectrometry (ICP-OES, PerkinElmer Optima). Thermogravimetric analysis was obtained by the Pyris Diamond TG/DTA (Perkin-Elmer) under constant air flow (50 mL/min) with a ramping rate of 5 ℃·min^{-1}.

Electrochemical Characterization: Electrochemical properties of VHCF were examined by the three-electrode system. The VHCF electrode, graphite plate and saturated calomel electrode (SCE, 0.241 V vs. standard hydrogen electrode, SHE) were used as working electrode, counter electrode, and reference electrode, respectively. To prepare the VHCF electrode: Typically, 70 wt% active material, 20 wt% carbon black and 10 wt% PVDF were mixed thoroughly by grinding before adding proper amounts of N-methyl pyrrolidone solution. Then the mixture was magnetically stirred overnight to form a homogeneous slurry. The slurry was drop-cast and spread on 1*1 cm^2 area of a carbon fiber paper (CFP). Afterwards, the VHCF @ CFP electrode was thoroughly dried in an oven at 80 ℃ overnight. The mass of active material was determined by comparing the CFP mass after and before VHCF loading then multiply the ratio of 0.7, and the average mass of active material herein was around 2.5 mg·cm^{-2}. During electrochemical tests, the VHCF @ CFP electrode was held by Pt clip at the plain end, and the slurry-coated region (1*1 cm^2) alone was immersed in the electrolytes (6.0 M H_2SO_4 or 0.5 M A_2SO_4, A=H^+, Li^+, Na^+, and K^+) with/without vanadium precursor additive. Cyclic voltammetry (CV) of the electrode was carried out by a CHI 630C potentiostat (CH Instruments, Inc.) at various scanning rates. Galvanostatic charge/discharge (GCD) measurements were performed by LAND CT2001A battery test system (Wuhan LAND electronics). Electrochemical Impedance Spectroscopy (EIS) was acquired from PGSTAT302N electrochemical potentiostat (Autolab) within the frequency range from 10^5 Hz to 0.01 Hz with amplitude of 5 mV.

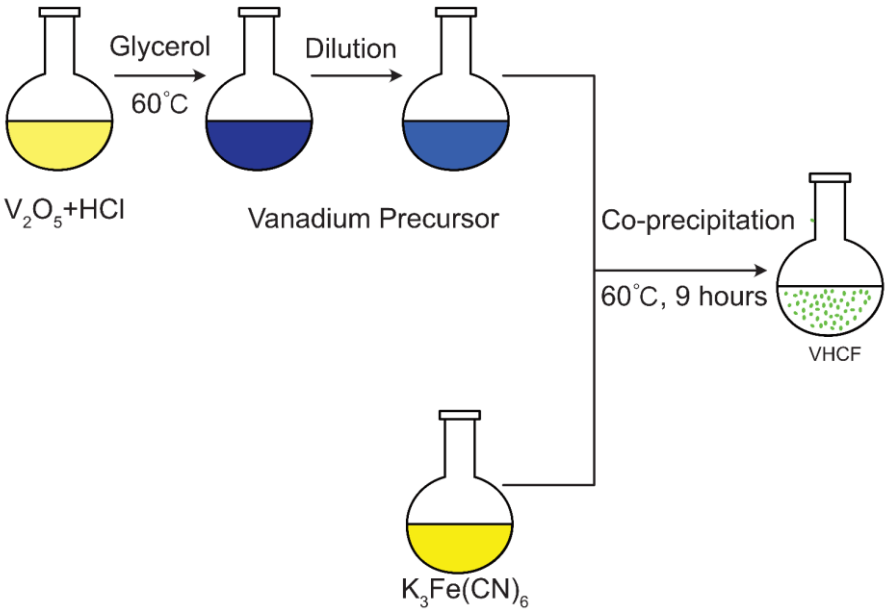

Figure S1. Schematic illustration of synthetic procedure for VHCF.

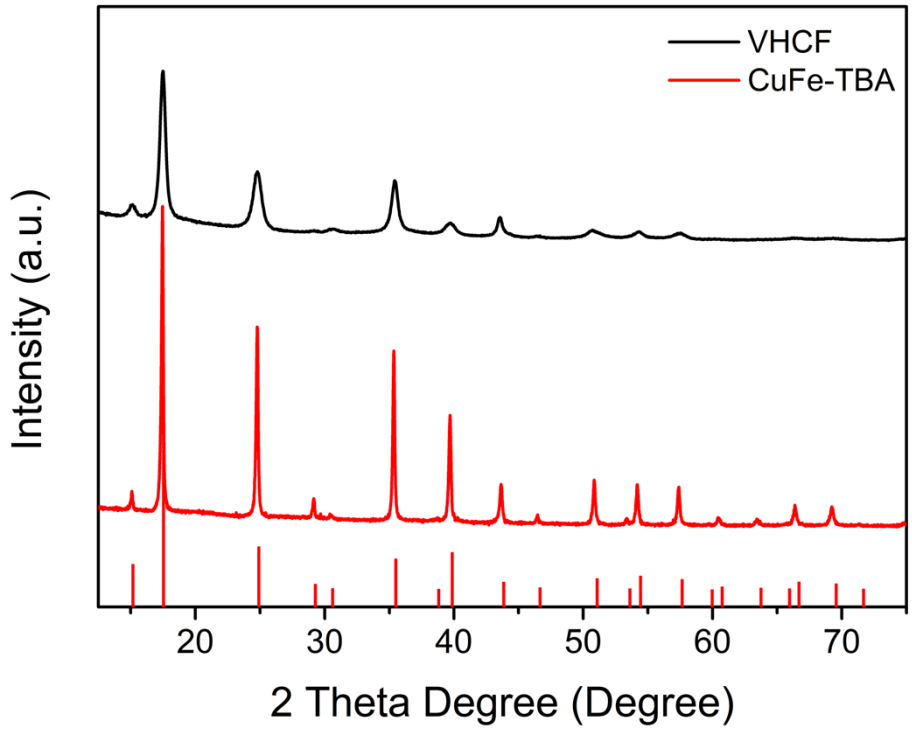

Figure S2. XRD patterns of as prepared VHCF and CuFe-TBA powders (ICDD ref. code: 01-070-2702). CuFe-TBA was synthesized according to a previous report,[2] and both samples were probed by the same apparatus with X-ray from Cu Kα radiation.

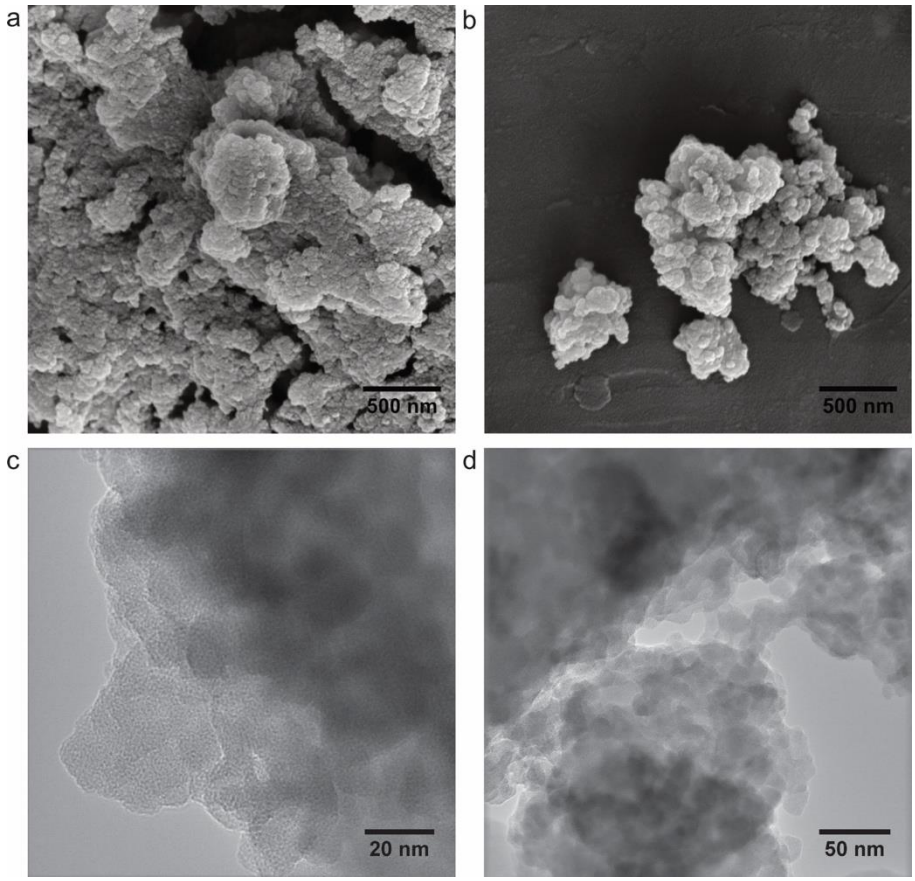

Figure S3. SEM images of VHCF under a) low-magnification and b) high-magnification. TEM images of VHCF under c) low-magnification and d) high-magnification.

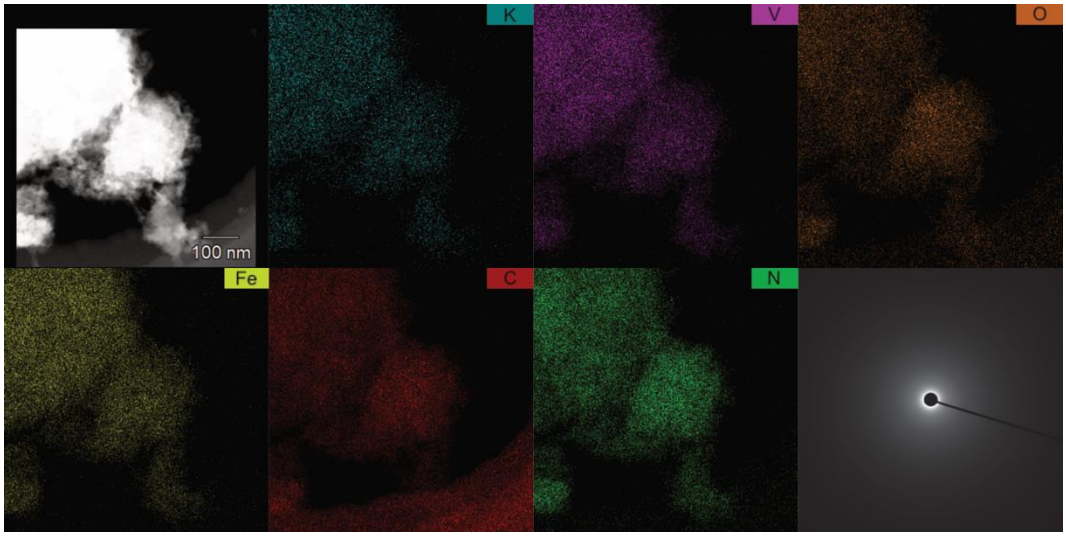

Figure S4. Diagram of STEM dark field image with corresponding element mapping results and selected-area electron diffraction (SAED) pattern.

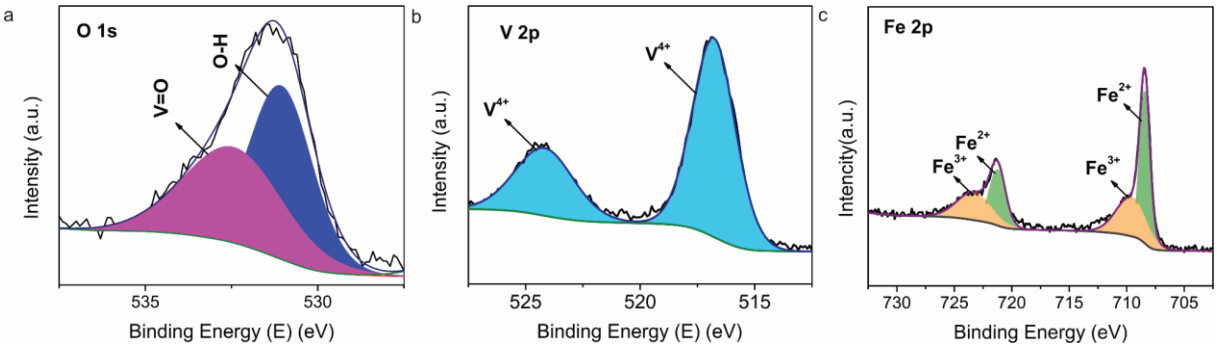

Figure S5. O 1s, V 2p and Fe 2p XPS core-level peaks recorded on the VHCF powder.

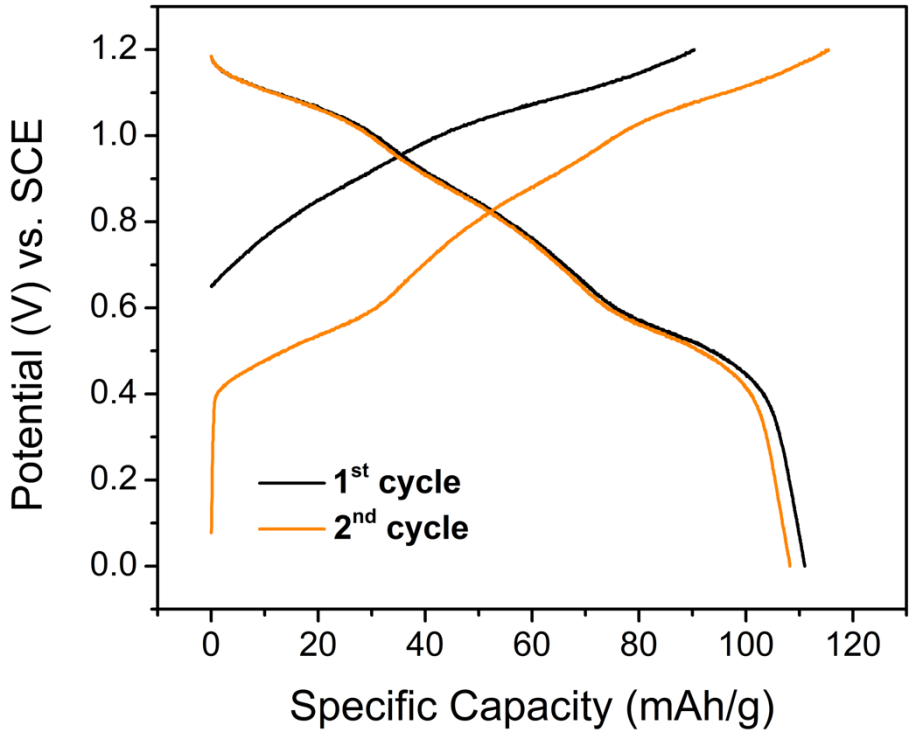

Figure S6. Charge/discharge profiles for first 2 cycles in 6.0 M H_2SO_4.

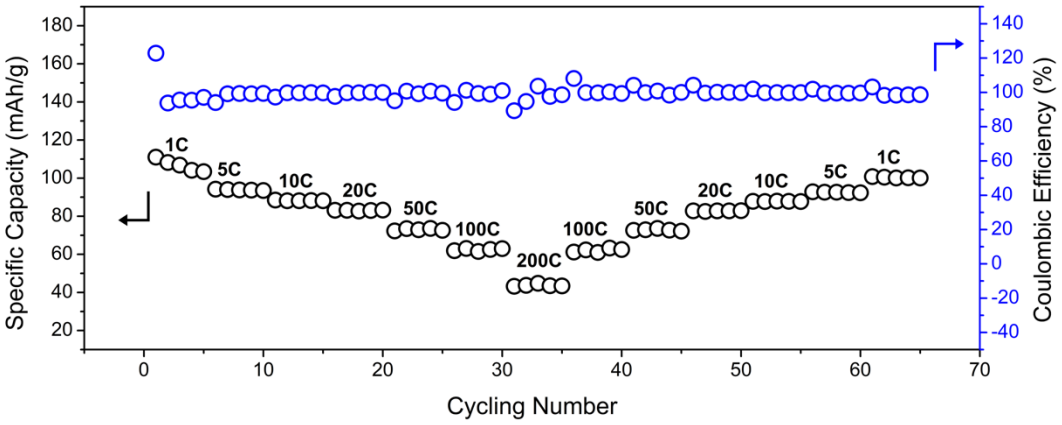

Figure S7. Rate performance of VHCF from 1 C to 200 C in 6.0 M H_2SO_4.

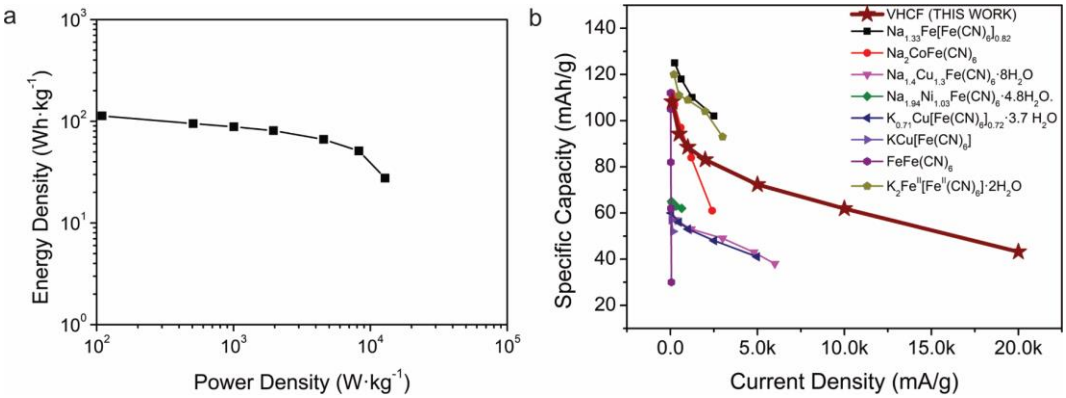

Figure S8. a) The Ragone plot of a half cell "proton battery", *i.e.* VHCF proton electrode. Energy-correlated values were calculated based on converted electrode potentials *v.s.* standard hydrogen electrode (SHE). b) Capacity versus current density plots for VHCF proton electrode as compared to performances of other PBA electrodes for aqueous sodium, potassium, and zinc ion batteries from main-stream reports.[3-10]

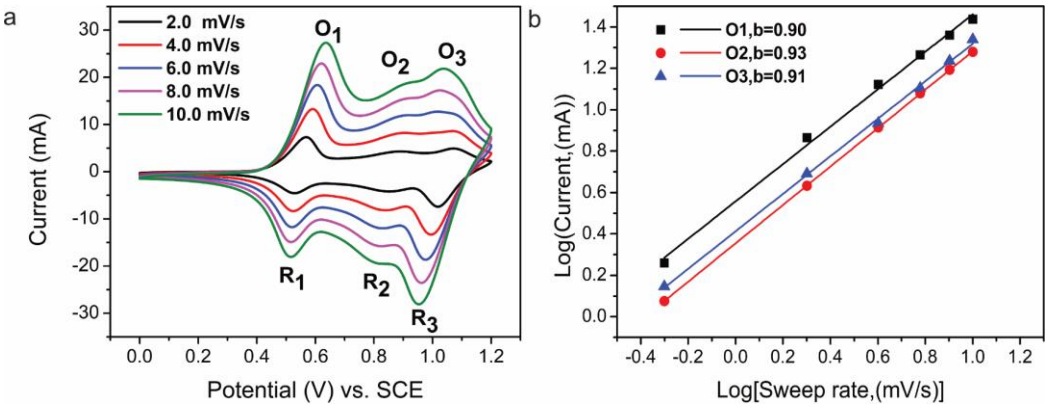

Figure S9. a) Cyclic voltammograms at scan rates from 2.0 $mV \cdot s^{-1}$ to 10.0 $mV \cdot s^{-1}$ with the potential range of 0.0-1.2V. b) b value derived from log (current) versus log (sweep rate) plots for oxidation peaks.

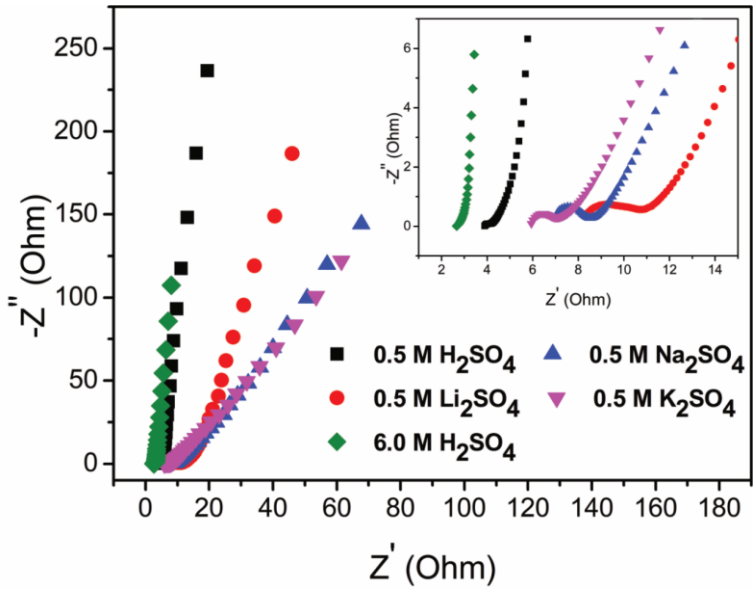

Figure S10. Nyquist plots of VHCF at open circuit voltage state in 0.5 M A_2SO_4 electrolytes (A=H^+, Li^+, Na^+, and K^+) and 6.0 M H_2SO_4 electrolytes, inset is the enlargement at high-frequency ranges.

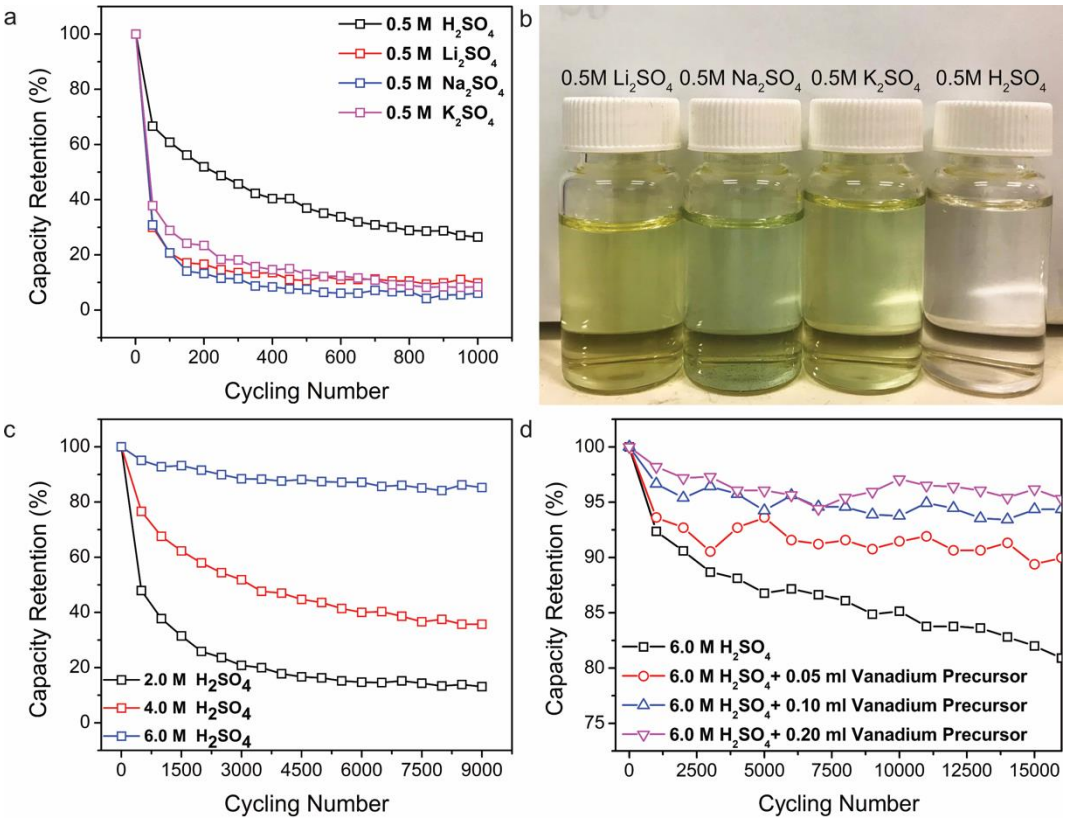

Figure S11. The capacity retention of VHCF at current density of 50 C a) in 0.5 M alkali metal sulphate solution and 0.5 M sulfuric acid and b) corresponding electrolyte solution after 1000 cycles; c) in acid solutions of different concentrations; d) in 6.0 M H_2SO_4 solution with different amount of vanadium precursor as additive.

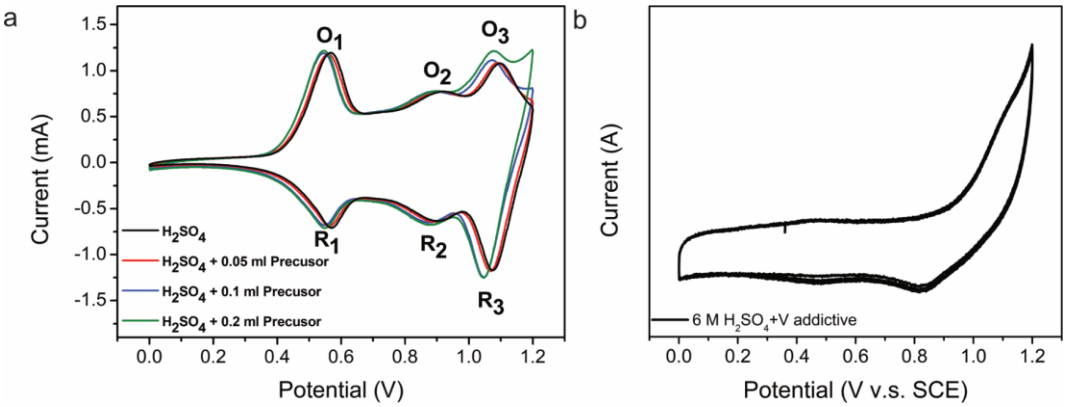

Figure S12. a) Cyclic voltammograms of VHCF at a scan rate of 1.0 $mV \cdot s^{-1}$ in 6.0 M H_2SO_4 with/without vanadium precursor as additive. b) Cyclic voltammograms of carbon fibre paper at a scan rate of 50 $mV \cdot s^{-1}$ in 6.0 M H_2SO_4 with vanadium precursor as additive.

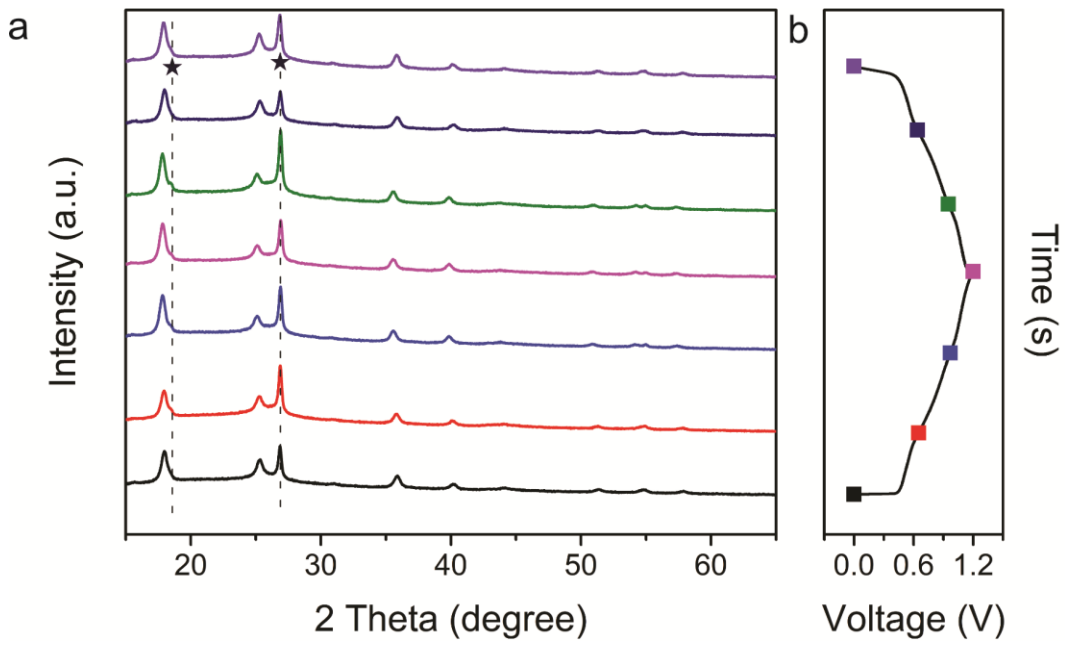

Figure S13. Full XRD patterns of VHCF electrode shown in Figure 3a. The "star" refers to signals from carbon fiber paper.

Table S1. Analysis of TGA results.

Temperature	Weight Loss (wt%)	Potential Product	Element/Groups in Material	Weight (wt%)
Stage 1	22.15 ± 0.01	H_2O	H_2O	22.15 ± 0.01
34.1(4) ℃ - 176.1(2) ℃				
Stage 2	7.28 ± 0.01	HCN	H_2O	1.61 ± 0.01
176.1(2) ℃ - 264.5(2) ℃			CN	7.10 ± 0.01
Stage 3	18.74 ± 0.01	$(CN)_2$	CN	18.74 ± 0.01
264.5(2) ℃ - 803.6(4) ℃				
Introduced oxygen of	-14.1 ± 0.9	VO_2	V	-10.3 ± 0.2
the whole process	(calculated)	Fe_2O_3	Fe	-6.10 ± 0.09
		K_2O	K	-0.59 ± 0.05
			O	2.9 ± 0.5

Note: negative value in this table refers to the amount of introduced oxygen (wt%) since TGA test was performed under airflow.

Table S2. Results of ICP-OES and summary of estimated weight percentages of elements or groups in VHCF.

	K	V	O	Fe	C≡N	H_2O
wt%(ICP)	2.9 ± 0.2	16.4 ± 0.2		14.2 ± 0.2		
wt%(TGA)						23.76 ± 0.02
wt%(Calculated)			2.9 ± 0.5		39.8 ± 0.5	

Table S3. Stability and capacity of PBAs electrode applied in the aqueous rechargeable batteries.

Materials	**Application Electrolyte**	**Current Density ($A \cdot g^{-1}$)**	**Initial Capacity ($mAh \cdot g^{-1}$)**	**Capacity Retention**	**Refs.**
VHCF	6.0 M H_2SO_4 + V additive	5	91.4	91.7%@25000	This Work
$Na_{1.33}Fe[Fe(CN)_6]_{0.82}$	1 M Na_2SO_4	1.25	108	83%@500	[3]
$Na_2CoFe(CN)_6$	1 M Na_2SO_4 + $CoSO_4$ additive	1.2	99.2	66.83%@2000	[4]
$Na_{0.4}(VO)_3[Fe(CN)_6]_2$	0.5 M Na_2SO_4 + 5 M H_2SO_4	0.11	91	60.4%@250	[11]
$K_{0.8}V_{1.8}O_xFe(CN)_6$	NaP-4.6	1.0	~69	93.1%@1000	[12]
$K_2NiFe(CN)_6 \cdot 1.2H_2O$	1 M KNO_3+ 0.01 M HNO_3	2.4	65.6	98.6%@5000	[13]
KFeMnHCF-3565	22 M KCF_3SO_3	13	94	90%@10000	[14]
$K_2Fe^{II}[Fe^{II}(CN)_6] \cdot 2H_2O$	0.5 M K_2SO_4	3	~103	81%@500	[5]
CuFe-TBA	2 M H_2SO_4	4.75	~73	~90%@10000	[2]

Reference

1. L. J. Small, H. D. Pratt, C. Staiger, R. I. Martin, T. M. Anderson, B. R. Chalamala, T. Soundappan, M. Tiwari and V. R. Subramanian, Vanadium Flow Battery Electrolyte Synthesis via Chemical Reduction of V_2O_5 in Aqueous HCl and H_2SO_4, Sandia National Lab.(SNL-NM), Albuquerque, NM (United States), 2017.
2. X. Y. Wu, J. J. Hong, W. Shin, L. Ma, T. C. Liu, X. X. Bi, Y. F. Yuan, Y. T. Qi, T. W. Surta, W. X. Huang, J. Neuefeind, T. P. Wu, P. A. Greaney, J. Lu and X. L. Ji, *Nat. Energy*, 2019, **4**, 123-130.
3. X. Wu, Y. Luo, M. Sun, J. Qian, Y. Cao, X. Ai and H. Yang, *Nano Energy*, 2015, **13**, 117-123.
4. T. Shao, C. Li, C. Liu, W. Deng, W. Wang, M. Xue and R. Li, *J. Mater. Chem. A*, 2019, **7**, 1749-1755.
5. D. Su, A. McDonagh, S. Z. Qiao and G. Wang, *Adv. Mater.*, 2017, **29**, 1604007.
6. X. Y. Wu, M. Y. Sun, Y. F. Shen, J. F. Qian, Y. L. Cao, X. P. Ai and H. X. Yang, *ChemSusChem*, 2014, **7**, 407-411.
7. X. Wu, Y. Cao, X. Ai, J. Qian and H. Yang, *Electrochem. Commun.*, 2013, **31**, 145-148.
8. D. W. Colin, A. H. Robert and C. Yi, *Nat. Commun.*, 2011, **2**, 550.
9. R. Trocoli and F. Lamantia, *ChemSusChem*, 2015, **8**, 481-485.
10. Z. Liu, G. Pulletikurthi and F. Endres, *ACS Appl. Mater. Interfaces*, 2016, **8**, 12158-12164.
11. J. H. Lee, G. Ali, D. H. Kim and K. Y. Chung, *Adv. Eng. Mater.*, 2017, **7**, 1601491.
12. P. Jiang, Z. Lei, L. Chen, X. Shao, X. Liang, J. Zhang, Y. Wang, J. Zhang, Z. Liu and J. Feng, *ACS Appl. Mater. Interfaces.*, 2019, **11**, 28762-28768.
13. W. Ren, X. Chen and C. Zhao, *Adv. Eng. Mater.*, 2018, **8**, 1801413.
14. L. Jiang, Y. Lu, C. Zhao, L. Liu, J. Zhang, Q. Zhang, X. Shen, J. Zhao, X. Yu and H. Li, *Nat. Energy.*, 2019, **4**, 495.